

# Supporting Information “Security Labeling and Optical Information Encryption Enabled by Laser-Printed Silicon Mie Resonators”

Sergey Syubaev,<sup>†,‡</sup> Ilya Gordeev,<sup>¶</sup> Evgeny Modin,<sup>§</sup> Vadim Terentyev,<sup>||</sup> Dmitriy  
Storozhenko,<sup>†</sup> Sergei Starikov,<sup>\*,⊥</sup> and Aleksandr A. Kuchmizhak<sup>\*,†,#</sup>

<sup>†</sup>*Institute of Automation and Control Processes, Far Eastern Branch, Russian Academy of  
Science, Vladivostok 690041, Russia*

<sup>‡</sup>*Far Eastern Federal University, Vladivostok 690091, Russia*

<sup>¶</sup>*Joint Institute for High Temperatures of RAS, Moscow, Russia*

<sup>§</sup>*CIC NanoGUNE BRTA, Avda Tolosa 76, 20018 Donostia-San Sebastian, Spain*

<sup>||</sup>*Institute of Automation and Electrometry, Siberian Branch, Russian Academy of Sciences,  
630090 Novosibirsk, Russia*

<sup>⊥</sup>*The Interdisciplinary Centre for Advanced Materials Simulation (ICAMS),  
Ruhr-Universität Bochum, Germany*

<sup>#</sup>*Pacific Quantum Center, Far Eastern Federal University, Russky Island, Vladivostok  
690922, Russia*

E-mail: sergei.starikov@icams.rub.de; alex.iacp.dvo@mail.ru

# 1. Laser ablation threshold of glass-supported $\alpha$ -Si film and additional SEM images showing film morphology upon single-pulse ablation at elevating fluence.

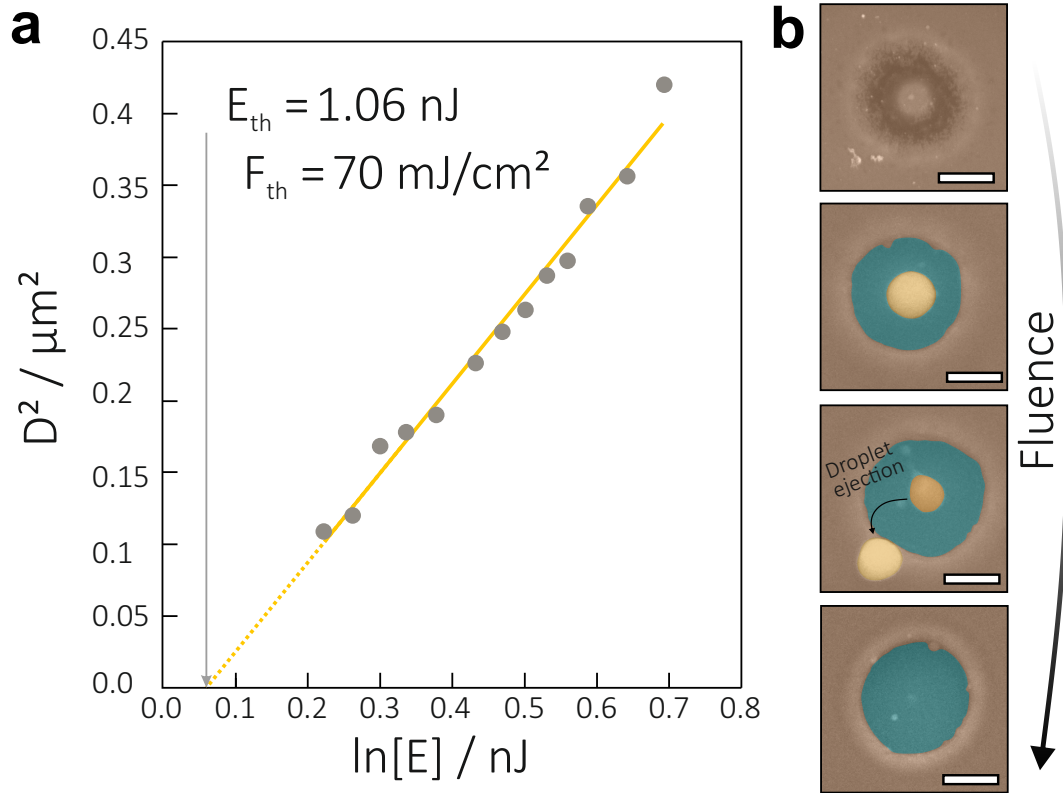


Figure S1 : (a) Squared diameter  $D^2$  of the through hole produced in the 24-nm thick  $\alpha$ -Si film under single-pulse exposure *versus* the natural logarithm of applied pulse energy  $\ln[E]$ . (b) Top-view SEM images showing evolution of the  $\alpha$ -Si film surface morphology upon increasing the pulse energy (fluence). Scale bar corresponds to 200 nm.

In this section, we provide the data of single-pulse ablation threshold of glass-supported 24-nm thick  $\alpha$ -Si film obtained by measuring the lateral size of the laser-induced surface modification (through hole) as a function of applied pulse energy. The data plotted as squared diameter of the through hole  $D^2$  *versus* natural logarithm of applied pulse energy  $\ln[E]$  are provided in Figure S1a revealing the characteristic energy deposition diameter  $D_{th} \approx 0.81$   $\mu\text{m}$  (slope of the linear fit) and the threshold pulse energy  $E_{th}=1.06$  nJ (intersection with

x axis). The resulting absorbed fluence can be estimated as  $F_{th}=4A \cdot E_{th}(\pi \cdot D_{th}^2)^{-1}= 70$  mJ/cm<sup>2</sup>, where A=0.35 is absorption coefficient of the film at 515 nm laser wavelength. Series of SEM images on Figure S1b reveals the key step of morphology evolution of the  $\alpha$ -Si film upon single-pulse ablation at elevating fluence  $F$  (pulse energy): (i) below-threshold redistribution of the material, (ii) rupture accompanied by formation of the hemispherical NP, (iii) partial ejection of the material stored in the NP and (iv) complete ejection of the molten material from the laser exposed area.

## 2. Dispersion curves of amorphous and crystalline Si considered in the electromagnetic simulations.

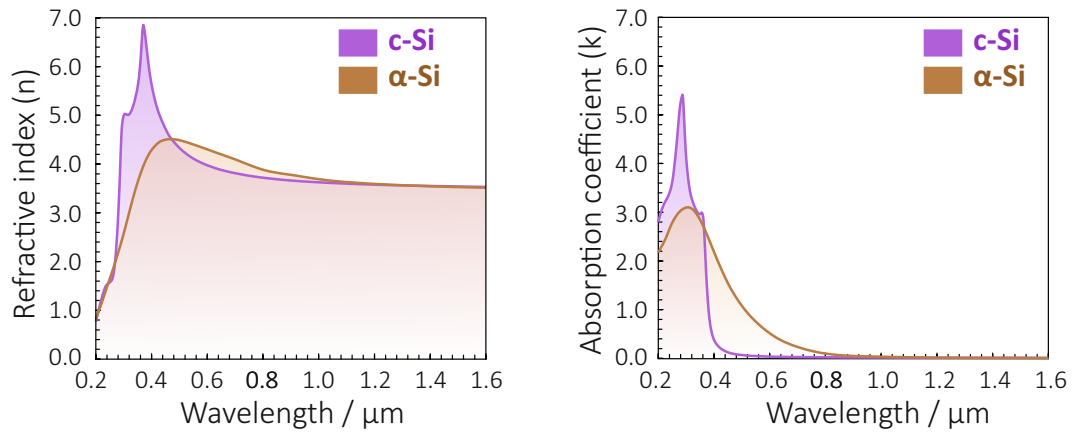


Figure S2 : Refractive index (n) and absorption coefficient (k) of amorphous and crystalline Si used for optical simulations).

### 3. Experimental setup for fabrication of the Si NP with adjustable focal spot size as well as additional SEM images illustrating fabrication process.

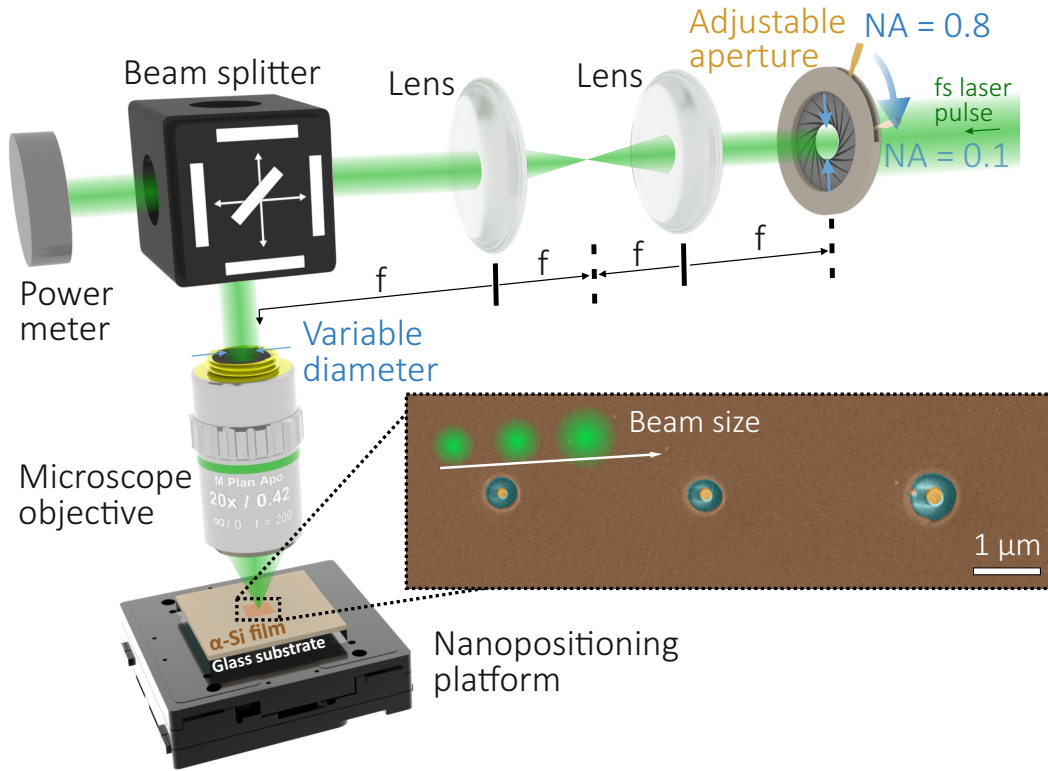


Figure S3 : Schematic of the experimental setup used to control the diameter of the laser-printed Si NP by tuning the size of the laser focal spot with an adjustable pinhole and a  $4f$ -optical system. The pinhole allows to reduce the laser beam diameter with respect to the entrance pupil of the microscope objective decreasing its effective numerical aperture. Inset: Top-view SEM image of the neighboring nanoparticle-embedded micro-holes produced at variable focal spot size.

#### 4. Measured and calculated laser-induced heating efficiency of Mie-resonant and non-resonant nanocrystalline Si NPs.

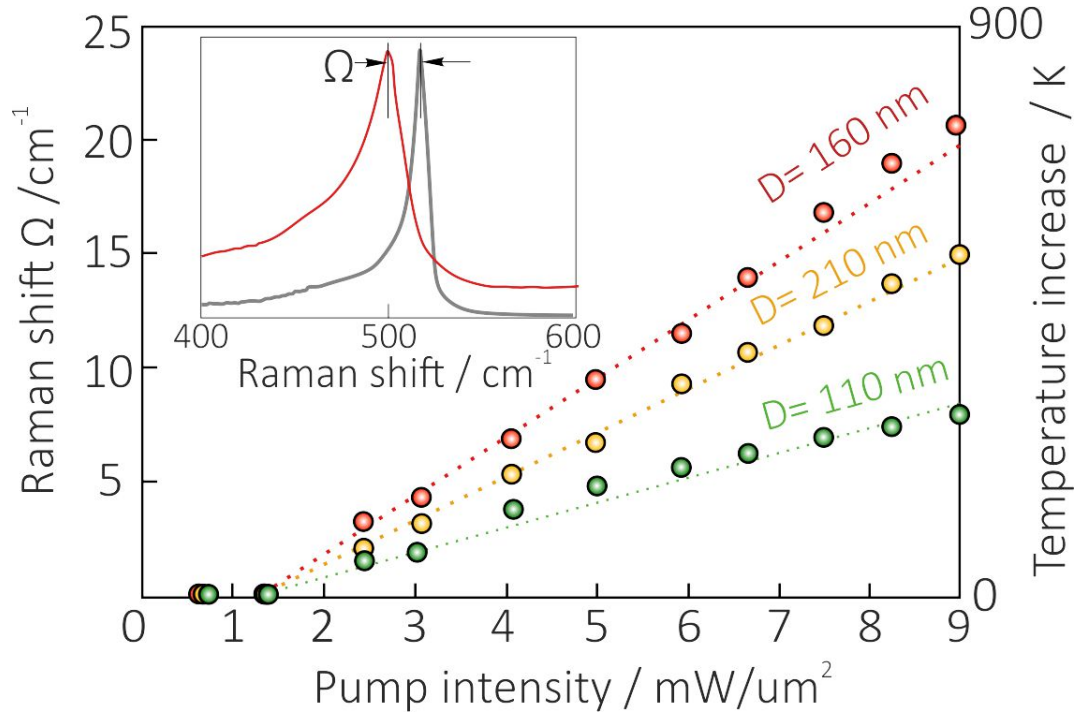


Figure S4 : Spectral shift  $\Omega$  of the Raman band corresponding to the nanocrystalline Si and the average temperature increase of the hemispherical Si NP versus pump laser intensity  $I$  measured for Mie-resonant ( $D=160$  nm) and non-resonant nanoparticles ( $D=110$  and  $210$  nm) at  $473$  nm laser pump. Inset shows representative Raman spectra of the cold and laser-heated Mie-resonant Si hemisphere.

## 5. Estimating resolution of the Si NP laser-printing process.

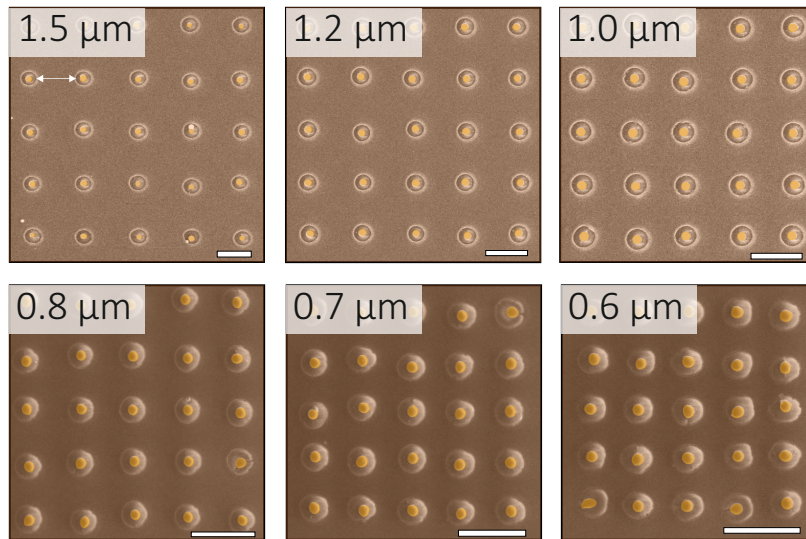


Figure S5 : Series of top-view SEM images showing  $5 \times 5$  arrays of Si NPs printed at variable period ranging from 1.5 to 0.6  $\mu\text{m}$ . Scale bar corresponds to 1  $\mu\text{m}$ .